Ab Initio Molecular Orbital Study of the $N(^2D) + H_2O$ Reaction

Yuzuru Kurosaki* and Toshiyuki Takayanagi

Advanced Science Research Center, Japan Atomic Energy Research Institute, Tokai-mura, Naka-gun, Ibaraki 319-1195, Japan

Received: September 16, 1998; In Final Form: November 11, 1998

Ab initio molecular orbital calculations have been carried out for the $N(^2D) + H_2O$ reaction. The reaction pathways were examined at the PMP4(full,SDTQ)/cc-pVTZ//MP2(full)/cc-pVTZ level of theory. It was calculated that the most stable intermediate product is $H_2NO(^2B_1)$ and the main product channels are $NH(^3\Sigma) + OH(^2\Pi)$, $HNO(^1A') + H$, and $NO(^2\Pi) + H_2$. It was found that a nonadiabatic process significantly contributes to the $NO(^2\Pi) + H_2$ channel. The contour plots of the potential surface were obtained at the FOCI/cc-pVTZ level in order to understand initial steps of the $N(^2D) + H_2O$ reaction: the N insertion into the OH bond, the N addition to the O atom, and the H atom abstraction by N. It was predicted that the N addition is the most favorable reaction pathway among these initial steps.

1. Introduction

Elementary reactions of the N atom with hydrocarbon molecules are regarded as important chemical processes in both the atmosphere of the earth and the interstellar space. However, these reactions have not been thoroughly examined both experimentally and theoretically, and available data for the reactions are very limited. In particular, experimental information on the detailed mechanisms of the elementary reactions are still insufficient since the reaction products have not been directly detected. For example, although Fell et al.[1] measured overall rate constants for the reactions of the electronically metastable nitrogen atom $N(^2D)$ with H_2, O_2, CO_2, CH_4, CF_4, etc., the reaction products were totally unidentified and hence the reaction mechanisms have been almost unclear. In fact, it is only recently that two research groups have succeeded in directly detecting the products of the N reactions. Umemoto and co-workers[2−5] have developed a laser photolysis technique and measured the nascent rotational and vibrational distributions of the NH molecule produced in the reactions of $N(^2D)$ with the H_2, H_2O, and saturated hydrocarbon molecules. Casavecchia and co-workers[6] have developed a crossed molecular beam technique and detected HCCN as a product of the $N(^2D) + C_2H_2$ reaction. These experiments are expected to give insights into the mechanisms of the N reactions. It is also very recently that we have theoretically studied the detailed mechanisms of the $N + H_2$,[7] $N + CH_4$,[8] $N + C_2H_2$,[9] and $N + C_2H_4$[10] reactions using ab initio molecular orbital (MO) theory.

In our previous studies[8−10] we have revealed some interesting aspects of initial steps for the reactions of the metastable nitrogen atom $N(^2D)$. In the $N(^2D) + CH_4$ reaction two reaction mechanisms can be considered as the initial step: insertion of $N(^2D)$ into the CH bond and abstraction of H by $N(^2D)$. It was predicted[8] that insertion is more likely to occur than abstraction, which leads to the formation of the intermediate product CH_3NH. This result is qualitatively consistent with the experiment of Umemoto et al.[3,4] In the $N(^2D) + C_2H_2$ reaction three mechanisms can be thought of as the first steps: addition of $N(^2D)$ to the CC π bond, insertion of $N(^2D)$ into the CH bond, and abstraction of H by $N(^2D)$. The ab initio MO results predicted[9] that the addition is the lowest reaction pathway and the main product is HCCN. This result is in agreement with the observation of Casavecchia and co-workers.[6] In the $N(^2D) + C_2H_4$ reaction the same three mechanisms as seen in the $N(^2D) + C_2H_2$ reaction are possible and addition of $N(^2D)$ to the CC π bond was again calculated to be the lowest reaction pathway.[10] One can thus conclude that for saturated hydrocarbon molecules $N(^2D)$ is likely to insert into the CH bond and for unsaturated hydrocarbon molecules $N(^2D)$ is likely to add to the CC π bond.

Elementary reactions of $N(^2D)$ with the H_2O molecule should also be one of the important chemical processes in the atmosphere of the earth. If this reaction is controlled by the same mechanism as predicted in the $N(^2D) + CH_4$ reaction, then insertion of $N(^2D)$ into the OH bond is dominant. However, since the O atom has lone pair electrons that should play a significant role, it is expected that addition of $N(^2D)$ to the O atom is another important pathway. Although several researchers[11−18] have already done theoretical calculations for the analogous system ($NH_2 + O$, $H_2 + NO$, etc.) to the $N(^2D) + H_2O$ reaction, initial steps, i.e., insertion, addition, and abstraction for the $N(^2D) + H_2O$ reaction, have never been discussed. In general it is not straightforward to theoretically predict the geometry of the transition states (TSs) which are saddle points located on the reaction pathway for some reactions. This is because TSs often originate from the avoided crossing of potential energy surfaces, which should be described with at least multireference wave functions even if one hopes to obtain a qualitative result. It is likely that multireference wave functions are required in order to treat the TSs for initial steps of the $N + H_2O$ reaction and that therefore calculations for the initial steps have long been prohibitive.

In this paper, first we report the results of ab initio MO calculations for the overall reaction of the $N(^2D) + H_2O$ system except initial steps. Next, we discuss the mechanisms of initial steps for this reaction on the basis of qualitative theoretical calculations with the configuration−interaction (CI) method.

* Author to whom correspondence should be addressed. E-mail: kurosaki@popsvr.tokai.jaeri.go.jp.

10.1021/jp9837378 CCC: $18.00
Published on Web 12/31/1998

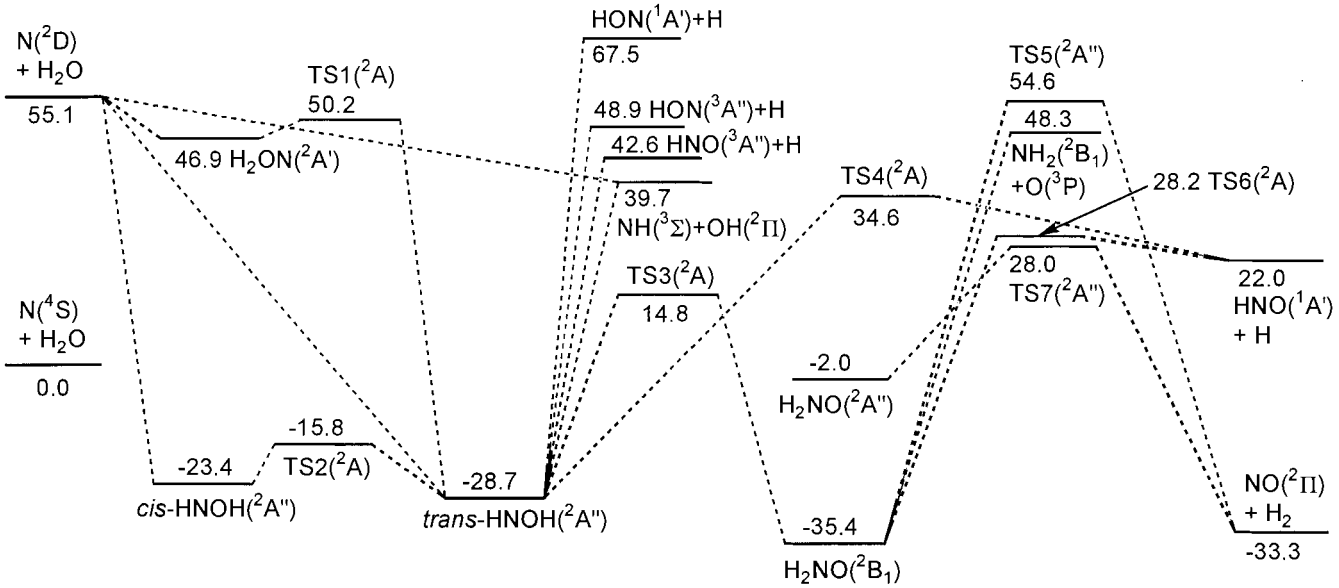

Figure 1. Potential energy diagram for the N(^{2}D) + H_2O reaction predicted at the PMP4(full,SDTQ)/cc-pVTZ//MP2(full)/cc-pVTZ + ZPE level. The unit is kcal mol^{-1}.

2. Methods of Calculation

Most ab initio MO calculations in this work were carried out using the GAUSSIAN 94 program.[19] Note that in calculations with this program the employed post Hartree−Fock (HF) levels of theory (MP2 and MP4) are based on spin-restricted and -unrestricted HF wave functions for closed- and open-shell systems, respectively. Geometry optimizations were done at the second-order Møller−Plesset perturbation (MP2(full))[20−22] level with the correlation consistent valence triple-ζ (cc-pVTZ) basis set of Dunning.[23] Harmonic vibrational frequencies were computed analytically at the MP2(full) level,[24] and the optimized geometries were characterized as potential minima or saddle points. Single-point calculations for the optimized geometries were also carried out at the MP4(full, SDTQ)[25,26] level of theory. Since spin-unrestricted MPn (UMPn) wave functions for open-shell molecules are in general not the eigenfunctions of spin operator $\mathbf{S}^2$, spin-projected UMPn (PMPn) wave functions[27] were calculated and the spin contamination was completely removed. Intrinsic-reaction-coordinate (IRC)[28−30] calculations were also performed at the MP2 level for several reaction pathways for which the TSs were found.

For initial steps of the N + H_2O reaction the first-order configuration interaction (FOCI) method was employed with the cc-pVTZ basis set using the HONDO7 program.[31] In the FOCI calculation the spin-restricted open-shell HF wave function was first obtained, and then the CI calculation with the single excitation was carried out, where the lower 4 and upper 61 orbitals were frozen in the total 88 orbitals and single excitation was considered in 23 orbitals. Thus we obtained potential surfaces for the four excited states as well as ground state that are 5-fold degenerate at the N(^{2}D) + H_2O asymptote.

3. Results and Discussion

A. Geometries and Energetics Except for Initial Steps. In this subsection computational results for reaction pathways from the first intermediate products to final products are reported. Initial-step mechanisms will be discussed in subsection C.

In Figure 1 is shown the diagram for the lowest doublet potential surface of the N(^{2}D) + H_2O reaction predicted at the PMP4(full,SDTQ)/cc-pVTZ//MP2(full)/cc-pVTZ + zero-point energy (ZPE) level of theory. Optimized geometries for intermediate products and TSs obtained at the MP2(full)/cc-pVTZ level are depicted in Figures 2 and 3, respectively. The harmonic vibrational frequencies calculated at the MP2(full)/cc-pVTZ level are given in Table 1. Total energy, ZPE, and expectation value of $\mathbf{S}^2$ are summarized in Table 2.

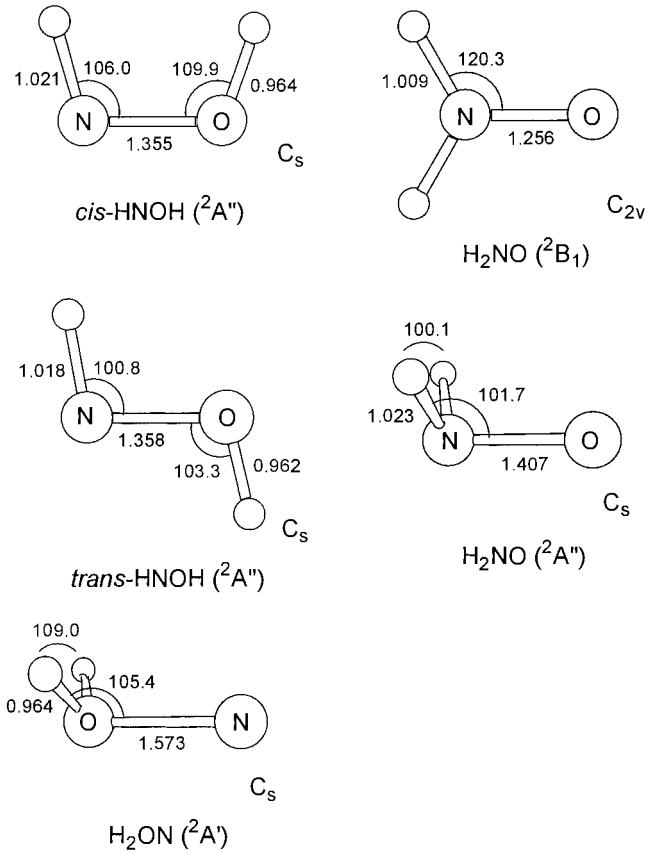

Figure 2. Optimized geometries for intermediate products predicted at the MP2(full)/cc-pVTZ level. Bond lengths and angles are given in Å and degree, respectively.

The initial steps of the N(^{2}D) + H_2O reaction can be characterized as the following three processes: the N insertion into the OH bond, the N addition to the O atom, and the H atom abstraction by N. The insertion produces *cis*-HNOH or

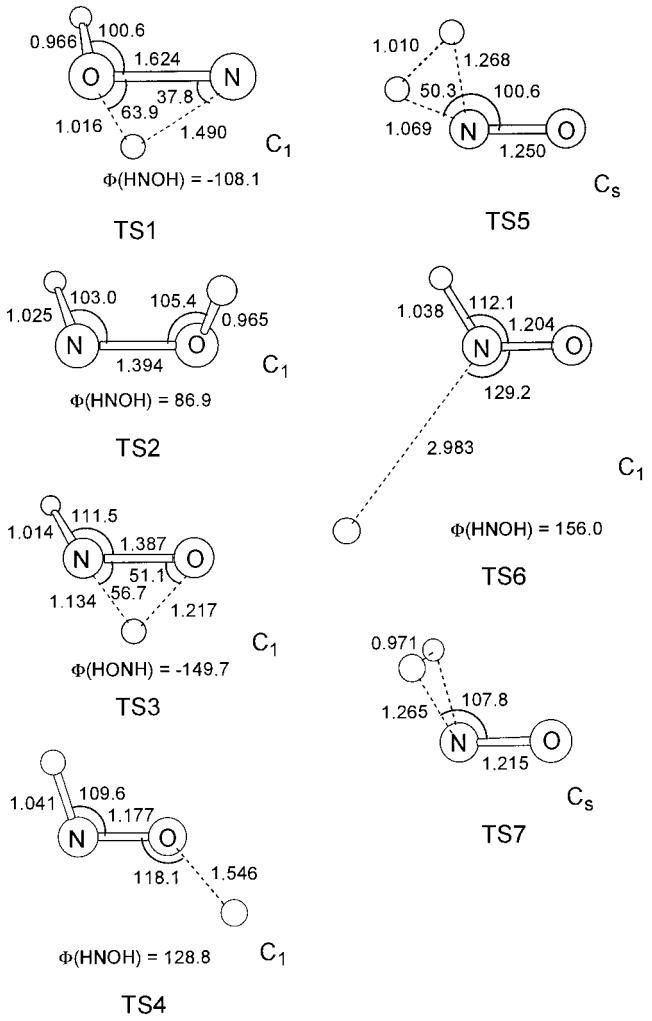

Figure 3. Optimized geometries for TSs predicted at the MP2(full)/cc-pVTZ level. Bond lengths and angles are given in Å and degree, respectively.

trans-HNOH which were calculated to be 78.5 and 83.8 kcal mol^{-1} lower in energy, respectively, than the N(^{2}D) + H_2O asymptote. This large exothermic energy suggests that the TS of the N insertion has an "early" character. The addition produces H_2ON which is seen to be quite unstable as compared to HNOH; H_2ON was predicted to be only 8.2 kcal mol^{-1} lower than the N(^{2}D) + H_2O asymptote. The abstraction directly produces one of the final products of the present system, NH($^3\Sigma$) + OH($^2\Pi$), which was calculated to be 15.4 kcal mol^{-1} lower in energy than the N(^{2}D) + H_2O asymptote. It is seen that NH + OH can be formed via another reaction pathway: the unimolecular dissociation of *cis*-HNOH or *trans*-HNOH. The barrier height for the *cis*-HNOH isomerization to *trans*-HNOH was estimated to be 7.6 kcal mol^{-1}, and that for the H_2ON isomerization to *trans*-HNOH to be 3.3 kcal mol^{-1}. Both TSs (TS1 and TS2) were predicted to have C_1 symmetry. The IRC analyses confirmed that TS1 and TS2 are located at the saddle points of the reaction pathways for the H_2ON → *trans*-HNOH and *cis*-HNOH → *trans*-HNOH isomerizations, respectively. It was calculated that *trans*-HNOH is 5.3 kcal mol^{-1} lower in energy than *cis*-HNOH and is 75.6 kcal mol^{-1} lower than H_2ON. It is thus considered that except for the H atom abstraction pathway all final products of the present reaction are generated from *cis*-HNOH or *trans*-HNOH.

There are several reaction pathways starting from *trans*-HNOH: one isomerization and five bond-rupture pathways. Note that upper four bond-rupture pathways [HON(^{1}A′) + H, HON(^{3}A″) + H, HNO(^{3}A″) + H, and NH + OH] from *cis*-HNOH are, of course, possible, although the dashed lines indicating reaction pathways are not explicitly drawn in Figure 1. However, bond rupture to HNO(^{1}A′) + H and isomerization to $H_2NO(^2B_1)$ directly from *cis*-HNOH may not be possible, which were shown by the IRC analyses as described below. It is seen that bond ruptures are energetically unfavorable compared to isomerization; the HON(^{1}A′) + H, HON(^{3}A″) + H, HNO(^{3}A″) + H, NH + OH, and HNO(^{1}A′) + H asymptotes were calculated to be 96.2, 77.6, 71.3, 68.4, and 50.7 kcal mol^{-1} higher in energy than *trans*-HNOH. TS4 was obtained as the saddle point of the reaction pathway for *trans*-HNOH → HNO(^{1}A′) + H. The barrier height of this bond rupture was predicted to be 63.3 kcal mol^{-1}. As shown in Table 2, the expectation value $\langle \mathbf{S}^2 \rangle$ for TS4 was estimated to be 1.160 for the UHF/cc-pVTZ wave function, which is considerably larger than the true doublet value 0.75. This suggests that the approximation based on the single-reference wave function, i.e., the UHF wave function, is inappropriate for TS4; however, the PMP4(full,SDTQ) values are considered to be reliable since it was shown[32] that projected MPn methods correctly describe the potential curves for bond ruptures where usual UMPn methods fail to be employed. It is also encouraging that TS4 was confirmed by the IRC analyses to be located at the saddle point of the isomerization pathway. Although one can imagine that there exist TSs for the bond ruptures: *trans*-HNOH → HON(^{1}A′) + H, HON(^{3}A″) + H, and HNO(^{3}A″) + H, we did not try to obtain these TSs since these reaction pathways are energetically unimportant. *Trans*-HNOH can isomerize into the $H_2NO(^2B_1)$ via TS3 with the barrier height being 43.5 kcal mol^{-1}. This isomerization is seen to be the most favorable reaction pathway that *trans*-HNOH can undergo. It was verified by the IRC analyses that TS3 is located at the saddle point of the isomerization pathway.

$H_2NO(^2B_1)$ was predicted to be the most stable intermediate product and can decompose into $NH_2(^2B_1)$ + O(^{3}P), HNO(^{1}A′) + H, and NO($^2\Pi$) + H_2, which were predicted to be 71.4, 57.4, and 2.1 kcal mol^{-1} higher in energy than $H_2NO(^2B_1)$. The $H_2NO(^2B_1)$ decomposition into HNO(^{1}A′) + H undergoes TS6 that was calculated to be 63.6 kcal mol^{-1} higher than $H_2NO(^2B_1)$. The IRC analyses again verified that TS6 is located at the saddle point of the decomposition pathway. In fact, we failed to find an IRC for the reaction pathway that correlates with the NO($^2\Pi$) + H_2 asymptote. Two C_s reaction pathways were examined; one has C_s symmetry with respect to the molecular plane of C_{2v} $H_2NO(^2B_1)$ ($C_s(1)$ pathway) and the other with respect to the plane perpendicular to the molecular plane of C_{2v} $H_2NO(^2B_1)$ ($C_s(2)$ pathway). Note that the electronic state of C_{2v} $H_2NO(^2B_1)$ is antisymmetric with respect to the $C_s(1)$ plane but symmetric with respect to the $C_s(2)$ plane. Therefore the electronic structure along the $C_s(1)$ pathway conserves the A″ state, and that along the $C_s(2)$ pathway conserves the A′ state. The $H_2NO(^2B_1)$ decomposition into NO($^2\Pi$) + H_2 via TS5 is symmetrically allowed since the electronic state of TS5 was calculated to be A″. Although the IRC calculation was not done to confirm that $H_2NO(^2B_1)$ connects with NO($^2\Pi$) + H_2 via TS5, we assumed that this is the case and drew lines connecting these stationary points in Figure 1. In fact, it was found that TS5 is not a true saddle point but has two imaginary vibrational modes with a′ and a″ symmetry as shown in Table 1. It is naturally expected that changing the TS5 geometry into the direction of the out-of-plane imaginary mode will lead to a TS with C_1 symmetry that connects $H_2NO(^2B_1)$ with NO($^2\Pi$) + H_2. Nevertheless, any

TABLE 1: Harmonic Vibrational Frequencies Calculated at the MP2(full)/cc-pVTZ Level

molecule	sym	frequency/cm^{-1}
	Fragment	
H_2 ($^1\Sigma_g$)	$D_{\infty h}$	4525 (σ_g)
NO ($^2\Pi$)	$C_{\infty v}$	3227 (σ)
NH ($^3\Sigma$)	$C_{\infty v}$	3414 (σ)
OH ($^2\Pi$)	$C_{\infty v}$	3837 (σ)
H_2O ($^1A_1$)	C_{2v}	1650 (a_1), 3874 (a_1), 3995 (b_2)
HNO (^{1}A′)	C_s	1501 (a′), 1592 (a′), 3047 (a′)
HNO (^{3}A″)	C_s	1175 (a′), 2181 (a′), 3414 (a′)
HON (^{1}A′)	C_s	1340 (a′), 1507 (a′), 3370 (a′)
HON (^{3}A″)	C_s	1157 (a′), 1268 (a′), 3759 (a′)
NH_2 ($^2B_1$)	C_{2v}	1556 (a_1), 3470 (a_1), 3571 (b_2)
	Intermediate Product (minimum)	
HNOH (^{2}A″)[a]	C_s	597 (a″), 1145 (a′), 1358 (a′), 1531 (a′), 3438 (a′), 3802 (a′)
HNOH (^{2}A″)[b]	C_s	778 (a″), 1158 (a′), 1288 (a′), 1594 (a′), 3495 (a′), 3838 (a′)
H_2ON (^{2}A′)	C_s	557 (a′), 757 (a′), 819 (a″), 1591 (a′), 3765 (a′), 3890 (a″)
H_2NO ($^2B_1$)	C_{2v}	255 (b_1), 1286 (b_2), 1527 (a_1), 1706 (a_1), 3516 (a_1), 3658 (b_2)
H_2NO (^{2}A″)	C_s	1032 (a′), 1201 (a′), 1224 (a″), 1585 (a′), 3393 (a′), 3476 (a″)
	Transition State (saddle point)	
TS1 (^{2}A)	C_1	1215*i*, 883, 1200, 1374, 3123, 3815
TS2 (^{2}A)	C_1	916*i*, 1020, 1222, 1445, 3385, 3808
TS3 (^{2}A)	C_1	918*i*, 1116, 1124, 1463, 3009, 3525
TS4 (^{2}A)	C_1	2201*i*, 664, 696, 1510, 1693, 3153
TS5 (^{2}A″)	C_s	2097*i* (a′), 1450*i* (a″), 819 (a′), 1536 (a′), 3090 (a′), 3290 (a′)
TS6 (^{2}A)	C_1	652*i*, 218, 666, 1342, 2488, 3238
TS7 (^{2}A″)	C_s	2017*i* (a′), 958 (a″), 1166 (a′), 1177 (a″), 1606 (a′), 2442 (a′)

[a] Cis isomer. [b] Trans isomer.

TABLE 2: Total Energy and Zero-Point Vibrational Energy (ZPE) for the MP2(full)/cc-pVTZ Geometries (hartree)

species	sym	MP2(full)	$\langle S^2\rangle$[a]	ZPE	PMP4(full,SDTQ)
		Fragment			
N (^{4}S)		−54.50681	3.756		−54.52447
N(^{2}D)		−54.44390	1.766		−54.43659
H (^{2}S)		−0.49981	0.75		−0.49981
O (^{3}P)		−74.96597	2.007		−74.98497
H_2 ($^1\Sigma_g$)	$D_{\infty h}$	−1.16465	0.0	0.01031	−1.17172
NO ($^2\Pi$)	$C_{\infty h}$	−129.71886	0.774	0.00735	−129.74844
NH ($^3\Sigma$)	$C_{\infty h}$	−55.12973	2.015	0.00778	−55.15232
OH ($^2\Pi$)	$C_{\infty h}$	−75.63127	0.756	0.00874	−75.65033
H_2O ($^1A_1$)	C_{2v}	−76.34664	0.0	0.02169	−76.34664
HNO (^{1}A′)	C_s	−130.29893	0.0	0.01399	−130.32854
HNO (^{3}A″)	C_s	−130.26543	2.035	0.01542	−130.29714
HON (^{1}A′)	C_s	−130.22164	0.0	0.01416	−130.25624
HON (^{3}A″)	C_s	−130.25267	2.022	0.01409	−130.28576
NH_2 ($^2B_1$)	C_{2v}	−55.78382	0.759	0.01959	−55.80706
		Intermediate Product (minimum)			
HNOH (^{2}A″)[b]	C_s	−130.87918	0.763	0.02705	−130.91374
HNOH (^{2}A″)[c]	C_s	−130.88844	0.763	0.02768	−130.92281
H_2ON (^{2}A′)	C_s	−130.76416	0.758	0.02593	−130.80062
H_2NO ($^2B_1$)	C_{2v}	−130.89965	0.766	0.02722	−130.93302
H_2NO (^{2}A″)	C_s	−130.84189	0.761	0.02713	−130.87967
		Transition State (saddle point)			
TS1 (^{2}A)	C_1	−130.75467	0.764	0.02368	−130.79309
TS2 (^{2}A)	C_1	−130.86495	0.762	0.02479	−130.89946
TS3 (^{2}A)	C_1	−130.81529	0.784	0.02332	−130.84910
TS4 (^{2}A)	C_1	−130.76053	1.160	0.01758	−130.81188
TS5 (^{2}A″)	C_s	−130.74399	0.790	0.01990	−130.78231
TS6 (^{2}A)	C_1	−130.73250	0.861	0.01812	−130.82268
TS7 (^{2}A″)	C_s	−130.78336	0.763	0.01674	−130.82149

[a] The expectation value of spin operator S^2 for the reference HF wave functions. [b] Cis isomer. [c] Trans isomer.

attempt to optimize the C_1 TS failed. It was also predicted that TS7 with C_s symmetry is located at the saddle point of the $C_s(2)$ pathway. The $H_2NO(^2B_1)$ decomposition into $NO(^2\Pi) + H_2$ via TS7 is symmetrically forbidden since the electronic state of TS7 was calculated to be A″. The IRC analyses demonstrated that TS7 is located at the saddle point of the reaction pathway that connects $H_2NO(^2A'')$ with the $NO(^2\Pi) + H_2$ asymptote; $H_2NO(^2A'')$ is located on an excited-state surface of H_2NO.

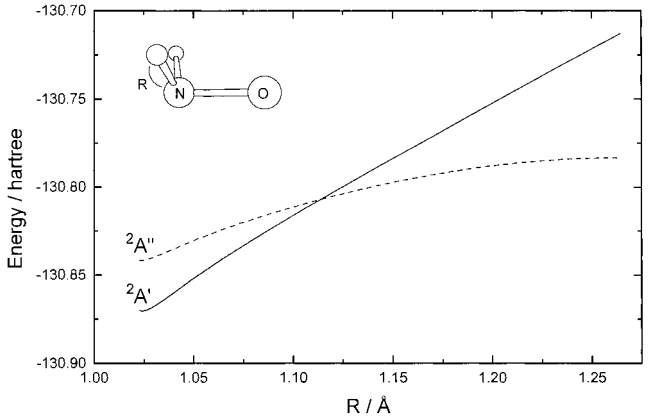

Figure 4. Potential energy profiles at the MP2(full)/cc-pVTZ level for the ^{2}A″ and ^{2}A′ states as a function of the internuclear distance (R) between N and H. The geometries along the IRC for the $H_2NO(^2A'')$ → TS7 reaction were employed.

It seems that in the ground-state N(^{2}D) + H_2O reaction there is no favorable reaction pathway leading to the $NO(^2\Pi) + H_2$ asymptote. The *cis*-HNOH → $NO(^2\Pi) + H_2$ reaction via a four-center TS is considered to be possible; however, attempts to optimize the TS resulted again in failure. We then compared the ^{2}A″ and ^{2}A′ potential curves along the $C_s(2)$ pathway from $H_2NO(^2A'')$ to TS7 in order to examine if avoided crossing occurs between the ^{2}A″ and ^{2}A′ surfaces. Note that the electronic state of ground-state $H_2NO(^2B_1)$ is ^{2}A′ with respect to the $C_s(2)$ plane. Figure 4 shows the ^{2}A″ and ^{2}A′ potential curves at the MP2(full)/cc-pVTZ level as a function of the internuclear distance (R) between N and H. Note that the geometries along the IRC calculated for $H_2NO(^2A'')$ → TS7 were employed in this calculation. The left and right ends of the potential curves correspond to the optimized geometries of $H_2NO(^2A'')$ and TS7, respectively. A crossing point is clearly seen around $R = 1.12$ Å. It is hence considered that avoided crossing occurs when

TABLE 3: Theoretical and Experimental Relative Energies for the $N(^2D) + H_2O$ System with Respect to the $NH_2(^2B_1) + O(^3P)$ Asymptote (kcal mol^{-1})

	ICCI[a]	CCSD(T)[b]	PMP4(full,SDTQ)[c]	expt[d]
$NH_2(^2B_1) + O(^3P)$	0.0	0.0	0.0	0.0
trans-HNOH($^2A''$)	−74.8	−77.3	−77.0	
cis-HNOH($^2A''$)	−69.6		−71.7	
$H_2NO(^2B_1)$	−79.8	−83.8	−83.7	
$H_2ON(^2A')$		−4.0	−1.4	
$NH(^3\Sigma) + OH(^2\Pi)$	−8.8	−10.2	−8.6	−5.7
$HNO(^1A') + H$	−22.7	−23.8	−26.3	−29.2
$NO(^2\Pi) + H_2$		−76.8	−81.6	−83.5
TS1(^2A)		1.5	1.9	
TS2(^2A)			−64.1	
TS3(^2A)	−31.8	−33.3	−33.5	
TS4(^2A)	−16.8	−15.4	−13.7	
TS5($^2A''$)	8.0		6.3	
TS6(^2A)	−22.3	−19.3	−20.1	
TS7($^2A''$)		−21.7	−20.3	

[a] The ICCI/cc-pVTZ//CAS/cc-pVDZ + ZPE method. Ref 14. [b] The CCSD(T)/6-311++G(3df,3pd)//CCSD(T)/6-311++G(d,p) + ZPE method. Ref 18. [c] ThePMP4(full,SDTQ)/cc-pVTZ//MP2/cc-pVTZ + ZPE method. Present work. [d] Ref 32.

symmetry of the system becomes C_1 from C_s. This suggests that $NO(^2\Pi) + H_2$ can be produced from ground-state $H_2NO(^2B_1)$ via a nonadiabatic transition from the $^2A'$ surface to $^2A''$.

In summary, the present calculations revealed that the main product channels of the ground-state $N(^2D) + H_2O$ reaction are $NH(^3\Sigma) + OH(^2\Pi)$, $HNO(^1A') + H$, and $NO(^2\Pi) + H_2$. It was predicted that a nonadiabatic transition from the $^2A'$ surface to $^2A''$ just before TS7 can lead to the $NO(^2\Pi) + H_2$ formation. The recent observation of Umemoto et al.[5] that the ground-state NH, OH, and H radicals were detected as products in the $N(^2D) + H_2O$ reaction is consistent with the present result; however, experiments to detect $NO(^2\Pi)$ or H_2 should be carried out in order to confirm the nonadiabatic reaction mechanism.

B. Comparison to Other Theoretical Results. Let us briefly review other theoretical results obtained at higher levels of theory for the system analogous to $N + H_2O$ and compare them to the present results. Walch[14] reported the computational results for the $NH_2 + O$ reaction; geometries were optimized by the CASSCF method with the cc-pVDZ basis set, and single-point energies were obtained by the internally contracted configuration interaction (ICCI) method with the cc-pVTZ basis set. Sumathi et al.[18] carried out calculations for the $H_2 + NO$ reaction at the CCSD(T) level using the 6-311++G(d,p) basis set for geometry optimizations and the 6-311++G(3df,3dp) basis set for single-point energy calculations. Available theoretical and experimental data for relative energies with respect to the $NH_2(^2B_1) + O(^3P)$ asymptote are given in Table 3. It is seen that the present results obtained at the PMP4(full,SDTQ)/cc-pVTZ//MP2(full)/cc-pVTZ + ZPE level agree fairly well with both the previous calculations and experiments. This encourages one to believe that the present level of theory is reliable enough to describe the $N + H_2O$ energetics. Although good agreement is seen in the energetics between the present and previous results, several inconsistent points are seen in the calculated geometries and harmonic vibrational frequencies, which will be described below.

First, some comments should be made on the geometrical structure of $H_2NO(^2B_1)$; in this work the $H_2NO(^2B_1)$ geometry was optimized to be planar at the MP2/cc-pVTZ level while it was optimized to be pyramidal at the CASSCF/cc-pVDZ level by Walch.[14] Several researchers[11,13,16,17] have thoroughly investigated the effects of electron correlation and basis set on the $H_2NO(^2B_1)$ geometry. It is thus widely accepted that the $H_2NO(^2B_1)$ geometry has a very small inversion barrier when taking electron correlation effects into account; however, the predicted inversion barrier is so small ($\sim$0.1 kcal mol^{-1}) that one can safely consider the geometry to be planar.

Second, Walch[14] considered TS5 (denoted by *sp5* in ref 14) to be the TS of the H_2 elimination from *cis*-HNOH. However, it was not confirmed by the IRC analysis that *sp5* is located on the reaction pathway of the H_2 elimination from *cis*-HNOH. In addition, the calculated OH bond length of *sp5*, 1.408 Å, seems slightly too long for the TS of the H_2 elimination. Therefore it may be natural to consider that TS5 is located on the reaction pathway of the H_2 elimination from $H_2NO(^2B_1)$ as mentioned in the previous subsection, although the IRC analysis for this pathway was not performed. A slight discrepancy is seen in the calculated values for harmonic vibrational frequency between TS5 and *sp5* (see Table 3 in ref 14). This may not be so surprising since in general calculated harmonic frequencies depend on the employed level of theory.

Third, although the calculated geometry and relative energy of TS3 in this work are consistent with the results of both Walch[14] and Sumathi et al.[18] (denoted by *sp1* in ref 14 and by **1/2** in ref 18), a discrepancy is seen in the calculated harmonic frequencies (see Table 3 in ref 14 and Table 2 in ref 18). The predicted imaginary frequency of TS3, 918*i* cm^{-1}, is only about half of both the imaginary frequencies of *sp1* and **1/2**. One of the reasons for this may be the difference in the employed methods and basis sets. As mentioned in the previous subsection, the IRC analyses confirmed that TS3 is located at the saddle point on the pathway of the *trans*-$HNOH(^2A'') \rightarrow H_2NO(^2B_1)$ reaction.

Fourth, the optimized geometry of TS6 in this work is seen to be slightly different from the results of Walch,[14] Soto and Page,[15] and Sumathi et al.[18] (denoted by *sp3* in ref 14 and by **1/8** in ref 18); the predicted NH-bond length, 2.983 Å, is considerably larger than their results. This may be due to a relatively large spin contamination; $\langle \mathbf{S}^2 \rangle$ for TS6 was estimated to be 0.861. Also, a small difference is found in the calculated harmonic frequencies. As mentioned in the previous subsection, however, TS6 was confirmed to be located at the saddle point of the $H_2NO(^2B_1) \rightarrow HNO(^1A') + H$ reaction.

Last, some comments should be made on the reaction pathway for the $H_2NO(^2B_1) \rightarrow NO(^2\Pi) + H_2$ reaction. As discussed above, the reaction is likely to occur via a nonadiabatic process and in the present calculation a saddle point could not be found. This is consistent with the fact that Walch[14] also failed to find a saddle point of this reaction. On the other hand, Sumathi et al.[18] optimized a TS denoted by **1/4,** which corresponds to TS7 in this work, and regarded **1/4** as the saddle point of the reaction. In this work, however, TS7 was proved to be the saddle point of the $H_2NO(^2A'') \rightarrow NO(^2\Pi) + H_2$ reaction by the IRC analyses as well as the examination of orbital symmetry.

C. Potential Energy Surface for Initial Steps. In this subsection, qualitative discussion based on the FOCI/cc-pVTZ method is given for initial steps of the $N(^2D) + H_2O$ reaction: the N insertion into the OH bond, the N addition to the O atom, and the H atom abstraction by N. First, the N atom was placed at several points in the H_2O plane, and second, it was placed in the plane which includes the OH axis and is perpendicular to the H_2O plane. Last, the N atom was placed at several points on the extended line of the OH axis. In these calculations the H_2O geometry was fixed at the MP2/cc-pVTZ geometry. Thus the potential energy surfaces for the initial steps of the $N(^2D) + H_2O$ reaction were calculated. Note that the ground-state potential surface for the $N(^2D) + H_2O$ system is 5-fold

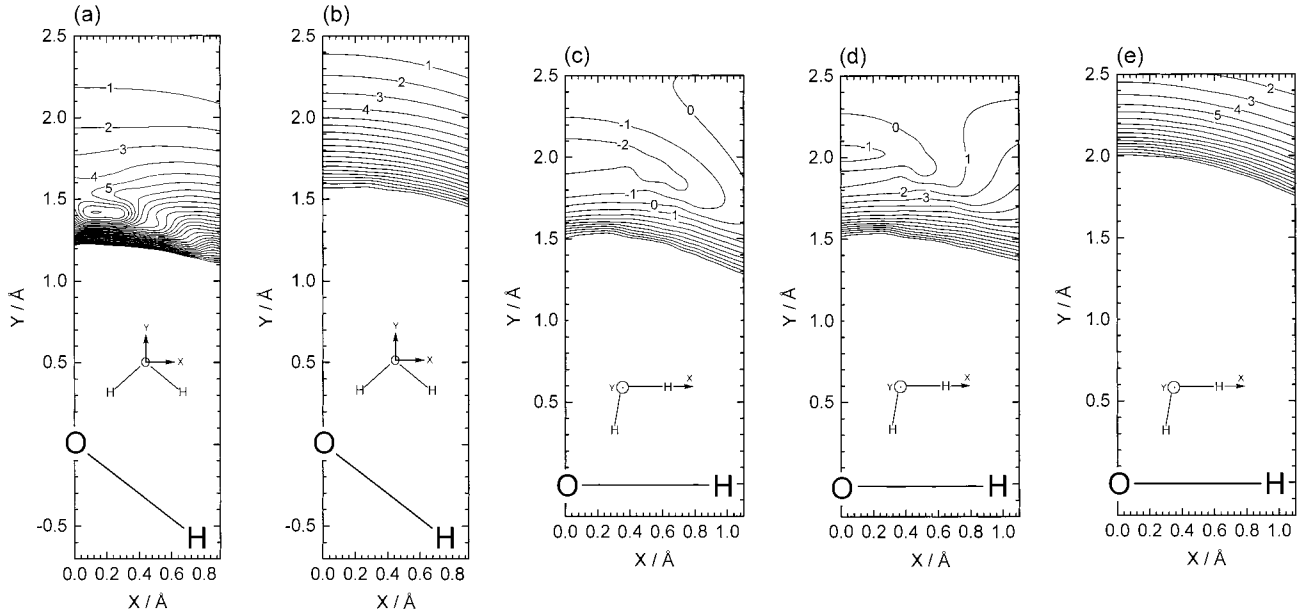

Figure 5. Contour plots of the potential energy surfaces at the FOCI/cc-pVTZ level for initial steps of the N(^{2}D) + H_2O reaction: (a) the ground state; (b) the first excited state; (c) the ground state; (d) the first excited state; (e) the second excited state. (a) and (b) are potentials for the N position in the H_2O plane, and (c) and (d) for the N position in the plane which includes the OH axis and is perpendicular to the H_2O plane.

degenerate at the reactant asymptote when spin−orbit coupling is not taken into consideration.

Figure 5a,b shows the contour plots of the ground- and first-excited-state potential surfaces, respectively, for the N position in the H_2O plane. In these figures the relative energy values are given in kcal mol^{-1} with respect to the reactant asymptote. In Figure 5a a repulsive character is seen in the ground-state potential surface for the N approach to H_2O in the H_2O plane; however, the N approach to the O atom is seen to be more likely than that to the OH bond. This suggests that the N addition to the O atom is slightly more favorable than the N insertion to the OH bond. As seen in Figure 5b, the first-excited-state potential is completely repulsive in all the region examined here. Similarly to the first-excited-state potential surface, the other three excited-state surfaces were found to be repulsive, although they are not shown.

Figure 5c−e shows the contour plots of the ground-state, first-excited-state, and second-excited-state potential surfaces, respectively, for the N position in the plane which includes the OH axis and is perpendicular to the H_2O plane. As depicted in Figure 5c, the ground-state potential surface exhibits an attractive character and a shallow minimum is seen on the *y*-axis. This means that the N addition to the O atom is more favorable than the N insertion to the OH bond. In Figure 5d a shallow minimum is also seen on the *y*-axis on the first-excited-state potential surface; however, the minimum is shallower than that seen on the ground-state potential surface. As seen in Figure 5e, the second-excited-state potential is completely repulsive in the entire region examined here. Similarly to this potential surface, the other two excited-state surfaces were found to be repulsive, although they are not shown. The computed potential surfaces shown in Figure 5 suggest that the reaction pathway of the N addition to the O atom is likely to be perpendicular rather than to be parallel to the H_2O plane. This is reasonable from the viewpoint of orbital interaction; the highest occupied molecular orbital of H_2O corresponds to the p orbital of O which is antisymmetric with respect to the H_2O plane, and it can interact with N effectively when N approaches perpendicularly to the H_2O plane. In addition, this is also consistent with the present

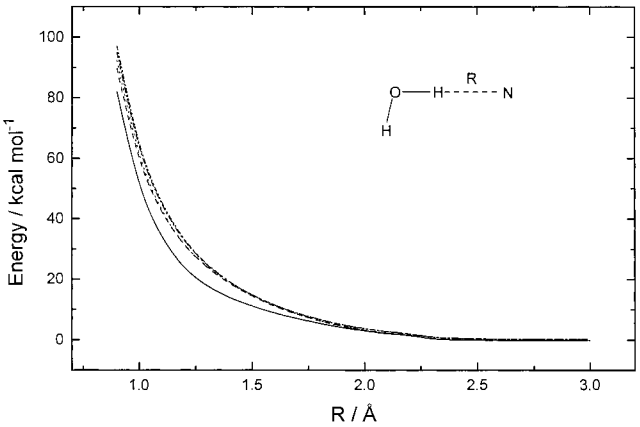

Figure 6. Potential curves at the FOCI/cc-pVTZ level for the H atom abstraction by N as a function of the internuclear distance (*R*) between N and H.

computational result that the MP2/cc-pVTZ geometry of H_2ON has a bend structure around the O atom as shown in Figure 2.

It is still unclear from the potential surfaces shown in Figure 5 whether the H atom abstraction by the N atom can occur, since the scanned region of the potential surface was limited. To examine the energetics for the H atom abstraction, the N atom was placed at several points on the extended line of the OH axis and five potential curves were obtained. Figure 6 shows the relative energies with respect to the reactant asymptote for the ground and four excited-state potentials as a function of the internuclear distance between N and H. It is clearly seen that all the potential curves are repulsive, suggesting that the H atom abstraction is unlikely to occur.

From the computational results obtained here at the FOCI/cc-pVTZ level, it is thought that both the insertion and abstraction have barriers, while the addition has no barrier. It is thus concluded that the N addition to the O atom is most likely to occur among the initial steps of the N(^{2}D) + H_2O reaction. However, since as shown in Figure 1 the barrier height of the $H_2ON(^2A')$ → *trans*-$HNOH(^2A'')$ reaction was calculated to be only 3.3 kcal mol^{-1} at the PMP4(full,SDTQ)/cc-pVTZ//MP2(full)/cc-pVTZ + ZPE level, it seems ambiguous whether

the initial $N(^2D)$ attack leads to the $H_2ON(^2A')$ formation or directly to the *trans*-$HNOH(^2A'')$ formation. Classical trajectory calculations using a reliable potential energy surface may therefore be needed to quantitatively discuss the initial-step mechanism, which is a future work.

4. Concluding Remarks

In this work, ab initio MO calculations have been carried out for the $N(^2D) + H_2O$ reaction. First, the reaction pathways except initial steps were examined at the PMP4(full,SDTQ)/cc-pVTZ//MP2(full)/cc-pVTZ level of theory. It was predicted that the most stable intermediate product is $H_2NO(^2B_1)$ and the main product channels are $NH(^3\Sigma) + OH(^2\Pi)$, $HNO(^1A') + H$, and $NO(^2\Pi) + H_2$. For the $NO(^2\Pi) + H_2$ channel a nonadiabatic process was found to be significant. The recent observation of Umemoto et al.[5] that the ground-state NH, OH, and H radicals were detected as products in the $N(^2D) + H_2O$ reaction is consistent with the present results. It is hoped that an experiment to detect $NO(^2\Pi)$ or H_2 as products of the $N(^2D) + H_2O$ reaction will be carried out soon in order to demonstrate the nonadiabatic reaction mechanism. Although the potential energy diagram obtained in this work is almost consistent with the previous higher-level calculations of other researchers, some minor discrepancies were found in geometries and harmonic frequencies. However, we believe that the reaction pathways predicted in this work are reliable since all the TSs except for TS5 were confirmed by the IRC analyses to be at the saddle points of the reaction pathways.

Next, the contour plots of the potential surface were obtained at the FOCI/cc-pVTZ level for initial steps of the $N(^2D) + H_2O$ reaction: the N insertion into the OH bond, the N addition to the O atom, and the H atom abstraction by N. It was then predicted that the N addition is the most favorable reaction pathway among the initial steps. However, since the barrier height of the $H_2ON(^2A')$ isomerization to *trans*-HNOH was calculated to be quite small, classical trajectory calculations using a reliable potential energy surface may be necessary in order to quantitatively examine whether the initial $N(^2D)$ attack leads to addition or insertion.

It is also of interest to study the dynamical aspects of the $N(^2D) + H_2O$ reaction. Umemoto et al.[5] observed that vibration of NH and rotation of both NH and OH are excited in the $N(^2D) + H_2O$ reaction. Dynamics calculations accounting for this dynamical behavior should be carried out in the future.

Acknowledgment. The authors would like to thank Prof. Hironobu Umemoto for helpful discussion.

Supporting Information Available: Cartesian coordinates (Å) for stationary points optimized at the MP2(full)/cc-pVTZ level (Table 4). Ordering information is given on any current masthead page.

References and Notes

(1) Fell, B.; Rivas, I. V.; McFadden, D. L. *J. Phys. Chem.* **1981**, *85*, 224.
(2) Umemoto, H.; Asai, T.; Kimura, Y. *J. Chem. Phys.* **1996**, *106*, 4985.
(3) Umemoto, H.; Kimura, Y.; Asai, T. *Chem. Phys. Lett.* **1997**, *264*, 215.
(4) Umemoto, H.; Kimura, Y.; Asai, T. *Bull. Chem. Soc. Jpn.* **1997**, *70*, 2951.
(5) Umemoto, H.; Asai, T.; Hashimoto, H.; Nakae, T. *J. Phys. Chem. A*, in press.
(6) Alagia, M.; Balucani, N.; Cartchini, L.; Casavecchia, P.; Volpi, G. G.; Sato, K.; Takayanagi, T.; Kurosaki, Y. Submitted for publication.
(7) Kobayashi, H.; Takayanagi, T.; Yokoyama, K.; Sato, T.; Tsunashima, S. *J. Chem. Soc., Faraday Trans.* **1995**, *91*, 3771.
(8) Kurosaki, Y.; Takayanagi, T.; Sato, K.; Tsunashima, S. *J. Phys. Chem. A* **1998**, *102*, 254.
(9) Takayanagi, T.; Kurosaki, Y.; Misawa, K.; Sugiura, M.; Kobayashi, Y.; Sato, K.; Tsunashima, S. *J. Phys. Chem. A* **1998**, *102*, 6251.
(10) Takayanagi, T.; Kurosaki, Y.; Sato, K.; Tsunashima, S. *J. Phys. Chem. A* **1998**, *102*, 10391.
(11) Soto, M. R.; Page, M.; Mckee, M. L. *Chem. Phys. Lett.* **1991**, *187*, 335.
(12) Soto, M. R.; Page, M. *J. Chem. Phys.* **1992**, *97*, 7287.
(13) Komaromi, I.; Tronchet, J. M. J. *Chem. Phys. Lett.* **1993**, *215*, 444.
(14) Walch, S. P. *J. Chem. Phys.* **1993**, *99*, 3804.
(15) Page, M.; Soto, M. R. *J. Chem. Phys.* **1993**, *99*, 7709.
(16) Cai, Z.-L. *Chem. Phys.* **1993**, *169*, 75.
(17) Ricca, A.; Weber, J.; Hanus, M.; Ellinger, Y. *J. Chem. Phys.* **1995**, *103*, 274.
(18) Sumathi, R.; Sengupta, D.; Nguyen, M. T. *J. Phys. Chem. A* **1998**, *102*, 3175.
(19) Frisch, M. J.; Trucks, G. W.; Schlegel, H. B.; Gill, P. M. W.; Johnson, B. G.; Robb, M A.; Cheeseman, J. R.; Keith, T.; Petersson, G. A.; Montgomery, J. A.; Raghavachari, K.; Al-Laham, M. A.; Zakrzewski, V. G.; Ortiz, J. V.; Foresman, J. B.; Cioslowski, J.; Stefanov, B. B.; Nanayakkara, A.; Challacombe, M.; Peng, C. Y.; Ayala, P. Y.; Chen, W.; Wong, M. W.; Andres, J. L.; Replogle, E. S.; Gomperts, R.; Martin, R. L.; Fox, D. J.; Binkley, J. S.; Defrees, D. J.; Baker, J.; Stewart, J. P.; Head-Gordon, M.; Gonzalez, C.; Pople, J. A. *GAUSSIAN 94*, Revision D.3; Gaussian, Inc., Pittsburgh, PA, 1995.
(20) Head-Gordon, M.; Pople, J. A.; Frisch, M. J. *Chem. Phys. Lett.* **1988**, *153*, 503.
(21) Frisch, M. J.; Head-Gordon, M.; Pople, J. A. *Chem. Phys. Lett.* **1990**, *166*, 275.
(22) Frisch, M. J.; Head-Gordon, M.; Pople, J. A. *Chem. Phys. Lett.* **1990**, *166*, 281.
(23) Dunning, T. H., Jr. *J. Chem. Phys.* **1989**, *90*, 1007.
(24) Head-Gordon, M.; Head-Gordon, T. *Chem. Phys. Lett.* **1994**, *220*, 122.
(25) Pople, J. A.; Binkley, J. S.; Seeger, R. *Int. J. Quantum Chem. Symp.* **1976**, *10*, 1.
(26) Krishnan R.; Pople, J. A. *Int. J. Quantum Chem.* **1978**, *14*, 91.
(27) Schlegel, H. B. *J. Chem. Phys.* **1986**, *84*, 4530.
(28) Fukui, K. *J. Phys. Chem.* **1970**, *74*, 4161.
(29) Gonzalez, C.; Schlegel, H. B. *J. Chem. Phys.* **1989**, *90*, 2154.
(30) Gonzalez, C.; Schlegel, H. B. *J. Phys. Chem.* **1990**, *94*, 5523.
(31) Dupuis, M.; Watts, J. D.; Villar, H. O.; Hurst, G. J. B. HONDO Version 7, *Comput. Phys. Comm.* **1989**, *52*, 415.
(32) Shlegel, H. B. *J. Chem. Phys.* **1986**, *84*, 4530.
(33) Afeefy, H. Y.; Liebman, J. F.; Stein, S. E. Neutral Thermochemical Data. In *NIST Chemistry WebBook*, NIST Standard Reference Database Number 69; Mallard, W. G., Linstrom, P. J., Eds.; National Institute of Standards and Technology, Gaithersburg MD 20899, March 1998; http://webbook.nist.gov.